research articles Journal of proteome research

Quantitative Proteomic Analysis of Tumor Reversion in Multiple Myeloma Cells

Feng Ge,[*,†] Liang Zhang,[‡] Sheng-Ce Tao,[§] Kaio Kitazato,[||] Zhi-Ping Zhang,[⊥] Xian-En Zhang,[⊥] and Li-Jun Bi[*,#]

Institute of Hydrobiology, Chinese Academy of Sciences, Wuhan, 430072, China, Division of Research, Singapore Health Research Facilities, Singapore 169611, Republic of Singapore, Shanghai Center for Systems Biomedicine, Shanghai Jiaotong University, 800 Dongchuan Road, Shanghai 200240, China, Department of Molecular Microbiology and Immunology, Nagasaki University, Nagasaki City, 1-14 Bunkyo-machi, Nagasaki 852-8521, Japan, State Key Laboratory of Virology, Wuhan Institute of Virology, Chinese Academy of Sciences, Wuhan 430071, China, and National Laboratory of Biomacromolecules, Institute of Biophysics, Chinese Academy of Sciences, Beijing 100101, China

Received September 29, 2010

Tumor reversion is defined as the process by which cancer cells lose their malignant phenotype. However, relatively little is known about the cellular proteome changes that occur during the reversion process. A biological model of multiple myeloma (MM) reversion was established by using the H-1 parvovirus as a tool to select for revertant cells from MM cells. Isolated revertant cells displayed a strongly suppressed malignant phenotype both in vitro and in vivo. To explore possible mechanisms of MM reversion, the protein profiles of the revertant and parental MM cells were compared using a quantitative proteomic strategy termed SILAC-MS. Our results revealed that 379 proteins were either activated or inhibited during the reversion process, with a much greater proportion of the proteins, including STAT3, TCTP, CDC2, BAG2, and PCNA, being inhibited. Of these, STAT3, which is significantly down regulated, was selected for further functional studies. Inhibition of STAT3 expression by RNA interference resulted in suppression of the malignant phenotype and concomitant down regulation of TCTP expression, suggesting that myeloma reversion operates, at least in part, through inhibition of STAT3. Our results provide novel insights into the mechanisms of tumor reversion and suggest new alternative approaches for MM treatment.

Keywords: Multiple myeloma (MM) • tumor reversion • stable isotope labeling by amino acids in cell culture (SILAC) • signal transducer and activator of transcription 3 (STAT3)

Introduction

Multiple myeloma (MM) is a malignant disorder of differentiated B cells (plasma cells). Clonal expansion of tumors results in excessive production of monoclonal immunoglobulin (Ig), a diagnostic feature of this disease.[1] MM can occur de novo or evolve from benign monoclonal gammopathy of undetermined significance (MGUS), and approximately 1% of individuals with MGUS develop MM each year.[2] MM is the second most common blood cancer and represents approximately 1% of all cancers and 2% of all cancer deaths.[3] Despite significant progress over the last 20 years, MM remains incurable, and the majority of patients eventually succumbs to the disease.[4] Cytogenetic techniques and molecular profiling technologies offer valuable tools for the study of tumor progression and have yielded new insights into the basic molecular events underlying the development of MM and the mechanisms of anticancer drug sensitivity/resistance.[5] By understanding the biology of MM and defining important potential therapeutic targets, effective new treatments can be developed to improve patient outcome.[6]

So far, the general approach used to understand the biology of MM has been to analyze the difference between normal and cancer cells, thus answering the question of how a normal plasma cell becomes a myeloma cell. However, these normal cell counterparts have never needed to acquire the ability to exit myeloma. A series of reports have suggested an alternative approach, namely, to analyze what it is that causes a malignant cell to revert.[7−12] It is postulated that the molecular mechanisms for overriding cancer are present in such revertant cells and that it is possible to determine the key factors that reverse malignancy which are selected for in cancer cells.[11,12] An understanding of how this reversion happens may lead to the identification of targets that were not previously revealed by comparing normal and tumor cells. Tumor reversion was first

* To whom correspondence should be addressed. Prof. Feng Ge. E-mail: gefeng@ihb.ac.cn. Phone/Fax: +86-27-68780500. Prof. Li-Jun Bi. E-mail: blj@sun5.ibp.ac.cn. Phone/Fax: +86-10-64871293.
† Institute of Hydrobiology, Chinese Academy of Sciences.
‡ Singapore Health Research Facilities.
§ Shanghai Jiaotong University.
|| Nagasaki University.
⊥ Wuhan Institute of Virology, Chinese Academy of Sciences.
Institute of Biophysics, Chinese Academy of Sciences.

10.1021/pr100992e

Published on Web 11/16/2010

discovered by Askanazy at the beginning of the 20th century[7] and later, in the 1950s, when Braun et al. described the recovery of tumor cells from the effects of the tumor-inducing principle in crown gall.[13,14] Pierce et al. then demonstrated that tumor cells can differentiate into benign tissues.[15] Seilern-Aspand described the induction of the differentiation of an epithelial tumor in newts and the regression of invasive tumors and metastasis.[16] Noda and colleagues have induced the reversion of *ras*-transformed cells and characterized genes such as *K-rev* and *RECK* which are involved in this process. This approach has led to the identification of potential drugs against cancer.[17−19] Telerman and Amson described an analysis of the reversion of some of the major cancers and demonstrated that down regulation of translationally controlled tumor protein (TCTP/*tpt1*) can induce tumor reversion.[11,12,20−22] Studying the rare events of tumor reversion and deciphering related pathways may lead to new avenues in cancer treatment.

The purpose of our work was to establish an experimental model for studying MM reversion, consisting of a parental human MM cell line and a cell line derived directly from it which exhibits suppressed malignancy. To obtain such a system we applied Telerman and Amson's approach; namely, we used the H1 parvovirus, a small single-stranded DNA virus, to select for revertant cells among RPMI8226 myeloma cells.[8−12] After the stable MM revertant cell line was established, quantitative proteome analysis was performed to explore the possible mechanism and potential effector proteins in MM reversion by examining differential protein expression between parental MM cells and revertant cells.

Proteomic techniques have recently become a powerful research tool for large-scale protein analysis. Stable isotope labeling by amino acids in cell culture (SILAC) is one of the most effective methods for the simultaneous detection of diverse changes in protein expression.[23] Its simplicity, inexpensiveness, and accuracy have led to SILAC being used more and more extensively in the life sciences.[24−28] In recent years, different proteomic approaches have been taken to investigate various aspects of MM and have provided new insights into the pathogenesis of MM.[29−31] In this study, the SILAC method was employed to compare the protein profiles of parental MM cells and revertants. In total, 379 differentially expressed proteins (DEPs) were identified, most of which interact in some way with STAT3, suggesting that the STAT3 pathway may play a vital role in myeloma reversion. Through functional studies, we also demonstrated that myeloma reversion operates, at least in part, through inhibition of the STAT3 pathway, which parallels the inhibition of the TCTP/*tpt1* pathway. Thus, MM reversion may take advantage of an existing dormant pathway in MM cells which, once activated, leads to the suppression of tumorigenicity.

Experimental Procedures

Selection of Revertant Cells. The human myeloma cell line RPMI8226 was purchased from American Type Culture Collections (ATCC) (Rockville, MD). Myeloma cells were routinely maintained in RPMI 1640 medium supplemented with 1% penicillin/streptomycin, 1 mmol/L L-glutamine, and 10% fetal bovine serum at 37 °C, 5% CO_2 in air. The RPMI8226 clone used initially went through two rounds of limited dilution to ensure that all cells were progeny of a single malignant cell. The wild-type H1 parvovirus was propagated in NBK-324K human embryonic kidney cells, purified on iodixanol gradient, and titrated using a plaque assay.[32] Different concentrations of the H1 parvovirus were used to infect RPMI8226 cells at a multiplicity of infection of 10−1000 plaque-forming units per cell using previously developed procedures.[7−12] The cytopathic effect of the virus caused massive cell death. After 10 weeks, the single clone which remained was expanded into a new culture and was infected with a second and then a third round of H1 parvovirus. The phenotype and tumorigenicity of this last culture, designated as RPMI8226-RC, were assessed in vitro and in vivo.

Characterization of MM Revertant Cells. DNA fingerprinting was performed as previously described.[33] Briefly, total genomic DNA was extracted from RPMI8226 and RPMI8226-RC cells using a Wizard Genomic DNA Purification Kit (Promega, Madison, WI) and then fingerprinted with a PowerPlex 1.2 System (Promega) using the following markers: D5S818, D13S317, D7S820, D16S539, vWA, TH01, Amelogenin, TPOX, and CSF1PO. PCR amplification was performed according to the manufacturer's instructions. Allele size was determined by electrophoresis of the PCR products in 6% denaturing polyacrylamide gels and was compared to ROX 500 size standards (Applied Biosystems, Foster City, CA), using an ABI 377 automated sequencer (Applied Biosystems). The fluorescent signals from the different-sized alleles were recorded and analyzed using GENESCAN version 3.1 and GENOTYPER version 2.1 (Applied Biosystems). Experiments were repeated three times.

To detect H-1 parvovirus DNA in RPMI8226-RC cells, PCR analysis was performed using the following primers: 5′-CTAG-CAACTCTGCTGAAGGAACTC-3′ and 5′-TAGTGATGCTGTTGCT-GTATCTGATG-3′, giving rise to a PCR product of 254 base pairs.[11]

To measure cell doubling time, cells were seeded in 24-well plates (3×10^5/well) on day 0, and a hemocytometric count was carried out daily. All measurements were carried out in triplicate. The cell doubling time was determined from cultures in the logarithmic growth phase.

For cell cycle analysis, cells were harvested, washed with ice-cold PBS, fixed with 70% ethanol for 1 h at 4 °C, and pretreated with RNase (Worthington, Lakewood, NJ) for 30 min at 37 °C. Cells were stained with propidium iodide (PI) (Sigma Chemicals, St. Louis, MO), and a cell cycle profile was determined using a FACScan flow cytometer (Becton Dickinson, San Jose, CA). Data analysis was carried out using WinMDI 2.8.

Apoptosis was detected by Annexin V/PI staining as previously described.[29]

For colony-forming efficiency analysis, soft agar (1.6 wt %/vol) was prepared by autoclaving Bacto-agar (DIFCO, Detroit, MI) in distilled water just before use. The bottom agar layer (2.1 mL/well) contained 1.6% agar:2 × RPMI/20% FBS:1 × RPMI/10% FBS without cells in a 1:1:1 volume ratio, giving a final agar concentration of 0.53%. The top agar layer (0.9 mL/well) contained 1.6% agar:2 × RPMI/20% FBS:1 × RPMI/10% FBS with cells in a 1:1:2 ratio, giving a final agar concentration of 0.4%. The number of cells plated for each clone was 5×10^2/mL. Plates were incubated at 37 °C with 5% CO_2 for 2 weeks, and the resulting colonies were stained with Giemsa and counted under a microscope. Results presented are the average of three independent experiments.

To measure the expression of various cellular markers, RPMI8226-RC revertant and parental RPMI8226 cells were collected and immunostained with specific monoclonal antibodies. The cell markers used were: CD5, CD10, CD11a, b, c, CD18, CD19, CD22, CD23, CD29, CD34, CD38, CD40, CD44, CD49d, e, CD54, CD56, CD58, CD138, and CD184 (BD Bio-

sciences). Samples were sorted on a FACScan flow cytometer (Becton Dickinson) and analyzed with WinMDI 2.8.

To detect λ free light chains (FLC) in the medium, the parental RPMI 8226 cell line and the corresponding revertant cells were maintained in culture for five days without feeding. The supernatant from each cell line was concentrated 10-fold using Amicon Ultra-15 centrifugal filtration units (Millipore, Billerica, MA). The detection of λ FLCs was carried out using IMMAGE reagents and an IMMAGE 800 nephelometer (Beckman Coulter, Brea, CA) according to the manufacturer's instructions. To detect cytoplasmic Ig (λ) expression, cells were washed in PBS and fixed using 4% paraformaldehyde for 30 min and then washed twice with PBS and incubated for 20 min with 0.1 M glycine in PBS to quench the fixed cells. Slides were immersed twice in PBS following cell permeabilization with 0.1% Triton X-100 for 5 min. After washing once in PBS, cells were incubated for 1 h with a mouse monoclonal Anti-Human Igλ (sc-69828, Santa Cruz) diluted 1:50 and stained with a Cy3-conjugated sheep antimouse IgG (H + L) Ab (Jackson ImmunoResearch, West Grove, PA), diluted 1:1000, for 45 min. The cells were then washed three times in PBS, and the slides were mounted with glycerol containing 4′-6′-diamidino-2-phenylindole (DAPI). The slides were examined using a Zeiss Axiovert 200 microscope (Zeiss, Thornwood, NY, USA).

For in vivo tumorigenicity, six- to eight-week-old male NOD/SCID mice were subcutaneously inoculated in the right flank with 3×10^7 RPMI8226-RC or RPMI8226 cells in 100 μL of RPMI-1640 medium, together with 100 μL of Matrigel basement membrane matrix (Becton Dickinson, Bedford, MA). Tumor size was measured in two dimensions using a caliper, and tumor volume was calculated using the formula $V = 0.5a \times b^2$, where a and b are the long and short diameter of the tumor, respectively. All studies published herein were carried out in strict accordance with the recommendations of the National Institutes of Health Guide for the Care and Use of Laboratory Animals. The protocol was approved by the Institutional Animal Care and Treatment Committee of the Singapore General Hospital.

Protein Analysis by SILAC Labeling. A SILAC Protein Quantitation Kit (Pierce Biotechnology, Rockford, USA) was used to differentially label RPMI8226-RC revertants and RPMI8226 parental cells according to the manufacturer's instructions. In brief, cells were grown in SILAC RPMI 1640 medium (Pierce Biotechnology, Rockford, USA) containing 10% v/v dialyzed FBS and 0.1 mg/mL of either heavy [$^{13}C_6$] or light [$^{12}C_6$] L-lysine (Pierce Biotechnology, Rockford, USA). Cells were propagated in SILAC medium for more than six generations to ensure nearly 100% incorporation of labeled amino acids. Cells were then washed three times with ice-cold washing buffer (10 μM Tris-HCl, 250 μM sucrose, pH 7.0), transferred to a clean 1.5 mL Eppendorf tube, and lysed with RIPA lysis buffer (50 mM Tris-HCl, 150 mM NaCl, 0.1% SDS, 1% NP-40, 0.5% sodium deoxycholate, 1 mM PMSF, 100 mM leupeptin, and 2 mg/mL of aprotinin, pH 8.0). Cellular debris was removed by centrifugation for 30 min at 13 200g at 4 °C. Protein concentrations were measured in duplicate using the RC DC protein assay (BioRad, Hercules, CA, USA) and confirmed by SDS-PAGE.

Protein Separation and In-Gel Digestion. Equal amounts of protein from RPMI8226-RC ($^{13}C_6$-lysine) and parental RPMI8226 cells ($^{12}C_6$-lysine) were mixed (100 μg in total), boiled in SDS-PAGE sample buffer, separated by 10% SDS-PAGE, and stained with Coomassie Brilliant Blue (CBB). An entire gel lane was cut into 30 sections for in-gel tryptic digestion. The excised sections were chopped into small particles, washed in water, and completely destained using 100 mM ammonium bicarbonate in 50% ACN. A reduction step was performed by addition of 100 μL of 10 mM DTT at 37 °C for 3 h. The proteins were alkylated by adding 100 μL of 50 mM iodoacetamide and allowed to react in the dark at 20 °C for 30 min. Gel sections were first washed in water and then acetonitrile and finally dried by SpeedVac for 30 min. Digestion was carried out using 20 μg/mL of sequencing grade modified trypsin (Promega, USA) in 50 mM ammonium bicarbonate. Sufficient trypsin solution was added to swell the gel pieces, which were kept at 4 °C for 45 min and then incubated at 37 °C overnight. The gels were extracted once with extraction buffer (67% acetonitrile containing 2.5% trifluoroacetic acid). The peptide extract and the supernatant of the gel slice were combined and then completely dried in a SpeedVac centrifuge.

Protein Identification and Quantification. Peptide mixtures from each of the gel slices were analyzed using an Agilent 6510 Q-TOF system coupled with an Agilent HPLC-Chip Cube MS interface (Agilent Technologies, Santa Clara, CA). The peptide mixture was first loaded onto the trapping column with a solvent mixture of 0.1% formic acid in CH_3CN/H_2O (2:98, v/v) at a flow rate of 4 μL/min. Peptides were then separated with a 90 min linear gradient of 5−60% acetonitrile in 0.1% formic acid at a flow rate of 300 nL/min. The Chip spray voltage (VCap) was set as 1950 V and varied depending on chip conditions. The temperature and flow rate of the drying gas were set at 325 °C and 4 L/min, respectively. Nitrogen was used as the collision gas, and the collision energy followed an equation with a slope of 3 V/100 Da and an offset of 2.5 V. MS/MS experiments were carried out in the data-dependent scan mode with a maximum of five MS/MS scans following each MS scan. The m/z ranges for MS and MS/MS were 300−2000 and 60−2000, and the acquisition rates were 6 and 3 spectra/s, respectively. Agilent MassHunter workstation software (version B.01.03) was used to extract the MS and MS/MS data. The data were converted to m/z data files with MassHunter Qualitative Analysis. Mascot Server 2.2 (Matrix Science, London, UK) was used for protein identification by searching the m/z data files against the Human IPI database version 3.36 (63 012 sequences). The maximum number of mis-cleavages for trypsin was set as one per peptide. Cys (+57.0215 Da, carbamidomethylation) was set as the fixed modification, whereas Met (+15.9949 Da, oxidation) and Lys (+6.0201 Da, SILAC heavy amino acid) were considered as variable modifications. The mass tolerances for MS and MS/MS were 50 ppm and 0.6 Da, respectively. Peptides identified with individual scores at or above the Mascot-assigned homology score ($p < 0.01$ and individual peptide score >30) were considered as specific peptide sequences. The false discovery rates (FDR) determined by decoy database searches were less than 1%. Proteins matching at least two reliable unique peptides were considered as positively identified proteins. All identified peptides were subjected to relative quantification analysis using the program Census.[34] Only proteins with a minimum of two quantifiable peptides were included in our final data set. The protein ratios were calculated from the average of all quantified peptides.

Protein Categorization and Network Construction. Differentially expressed proteins (DEPs) were classified based on the PANTHER (Protein ANalysis THrough Evolutionary Relationships) system (http://www.pantherdb.org), which classifies genes and proteins by their functions.[35] A DEP interaction

network was generated with Pathway Studio version 5.0 (Ariadne Genomis, Rockville, MD) and the Resnet 5 database.[36] Common downstream targets or upstream regulators of multiple proteins were identified using this software, which facilitated the process of selecting key factors and potential mechanisms from the large number of proteins.

Western Blotting. Protein extracts (30 μg) prepared with RIPA lysis buffer (50 mM Tris-HCl, 150 mM NaCl, 0.1% SDS, 1% NP-40, 0.5% sodium deoxycholate, 1 mM PMSF, 100 mM leupeptin, and 2 mg/mL of aprotinin, pH 8.0) were resolved on a 10% SDS-PAGE gel and transferred to an Immobilon-P PVDF transfer membrane (Millipore, Bedford, MA) by electroblotting. After blocking with 5% nonfat milk, membranes were probed with goat anti-SRP54 polyclonal, goat anti-H2AFX polyclonal, mouse anti-HSPA1A monoclonal (Santa Cruz Biotechnology, Santa Cruz, CA), mouse anti-PSMC5 polyclonal, goat anti-BAG2 polyclonal, rabbit anti-TCTP polyclonal, rabbit anti-PCNA polyclonal, mouse anti-STAT5A monoclonal, rabbit anti-CDC2 polyclonal (Abcam Inc., Cambridge, MA), rabbit anti-pY705-STAT3 polyclonal, rabbit anti-eIF5 polyclonal, rabbit anti-PLK1 polyclonal, rabbit anti-YWHAQ polyclonal, rabbit anti-STAT3 polyclonal, rabbit antivimentin polyclonal (Cell Signaling, Danvers, MA), rabbit anti-S100A11 polyclonal, and rabbit anti-HSPB1 polyclonal antibodies (Abgent, San Diego, CA). Blots were then incubated with peroxidase-conjugated antimouse, antirabbit, or antigoat IgG (KPL, Gaithersburg, Maryland) for 1 h at room temperature at a 1:1000 dilution and then developed using a SuperSignal West Pico kit (Pierce Biotechnology, Rockford, IL). Immunoblots were scanned using an Image Scanner (GE healthcare, Uppsala, Sweden). Blot densitometry analysis was performed using ImageJ (National Institutes of Health).

STAT3 Small Interfering RNA Silencing. STAT3 gene silencing was achieved by transfecting RPMI8226 cells with a plasmid in which the cloned DNA fragment acts as a template for the synthesis of small interfering RNA molecules using the siSTRIKE U6 Hairpin Cloning System (Promega, Madison, WI). The siRNA which targeted the STAT3 sequence corresponded to nucleotides 823 to 841 of human STAT3.[37] A negative control scrambled siRNA (TTCTCCGAACGTGTCACGT), which has no significant homology to human gene sequences, was used as a control. Oligonucleotides were cloned in the pSiStrike vector, containing a puromicin-resistant gene according to the manufacturer's instructions. The resulting pSiStrike/STAT3 and pSiStrike/control vectors were purified and used to transfect the RPMI8226 cell line. Cells were grown to 60−80% confluence and then transfected with 2 μg of the pSiStrike/STAT3 or control vector (pSiStrike/control) using FuGENE6 (Roche Molecular Biochemicals) according to the manufacturer's instructions. Transfected cells were selected for puromicin resistance for 2 weeks. Two clones were selected from pSiStrike/control transfected RPMI8226 cells (designated as MM-KD1, MM-KD2) and one from pSiStrike/control transfected RPMI8226 cells (designated as MM-NC).

Characterization of STAT3 Knock-Down MM Cells. Changes in STAT3 mRNA levels were determined by quantitative real-time PCR (qRT-PCR). RNA was isolated from the parental RPMI8226 cells, two stable STAT3 knock-down clones, MM-KD1 and MM-KD2, and one stable negative control STAT3 clone, MM-NC, using TRIzol Reagent (Invitrogen). cDNA was synthesized using SuperScript III First-Strand Synthesis Systems for RT-PCR (Invitrogen). An amount of 50 ng of cDNA was amplified and quantified by qRT-PCR with STAT3 and GAPDH TaqMan Gene Expression Primer sets (Applied Biosystems).

Changes in STAT3 and TCTP/*tpt1* protein levels were determined by Western blotting, as described above.

Cell doubling time, cell cycle, apoptosis, colony assays, and in vivo tumorigenicity were measured as described above.

Statistical Analysis. All data are expressed as means ± standard deviation. The statistical significance of in vitro data was determined by the Student's *t* test (two-tailed), while the

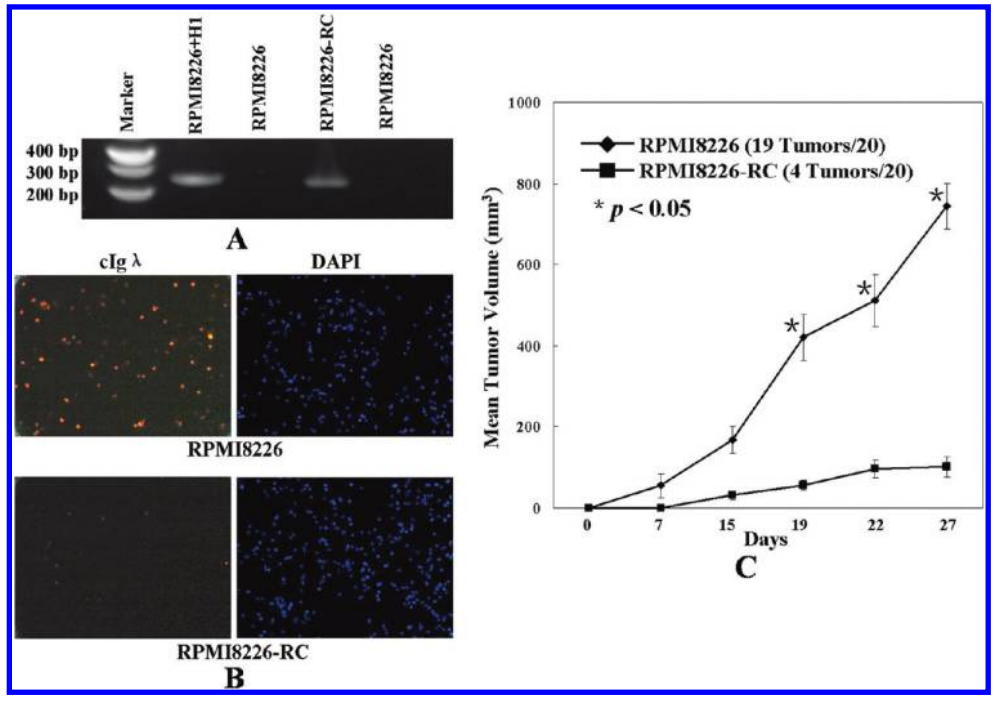

Figure 1. Characterization of MM revertant cells. (A) PCR analysis of a region of 254 base pairs of the H-1 parvovirus in RPMI8226 uninfected, in parvovirus infected (RPMI8226 + H1), and in the revertant RPMI8226-RC cells. (B) Cytoplasmic Igλ staining of RPMI 8226 and RPMI8226-RC cells. DAPI staining was used to stain nuclei. (C) In vivo tumorigenicity after injection of 3×10^7 RPMI8226 or RPMI8226-RC cells per site.

Table 1. Short Tandem Repeat (STR) Analyses of RPMI8226 and RPMI8226-RC Cells

locus	RPMI8226	RPMI8226-RC
Amelogenin	X, Y	X, Y
CSF1PO	12	12
THO1	8	8
TPOX	8, 11	8, 11
vWA	16, 18	16, 18
D13S317	11	11
D16S539	9	9
D5S818	11, 13	11, 13
D7S820	9, 10	9, 10

Table 2. Summary of the Growth Properties of RPMI8226 and Revertant RPMI8226-RC Cells[a]

	RPMI1640/10% FBS		soft agar	annexin V/PI staining	
cell	doubling time (h)	G1/S/G2/M phase, %	CFE (%)	apoptotic ratio (%)	λ FLC (mg/dl)
RPMI8226	36	55/31/14	25 ± 3.2	2.7 ± 0.9	177 ± 31
RPMI8226-RC	38	57/28/15	3.2 ± 1.1	3.5 ± 0.8	46 ± 11

[a] CFE, colony-forming efficiency; FBS, fetal bovine serum; FLC, free light chain.

significance of differences between the median values of in vivo data was determined using the two-tailed Mann−Whitney test. Statistical significance was assigned if $p < 0.05$.

Results

Derivation of the MM Revertant Cell Line. To obtain the myeloma reversion model, we used the approach as described by Telerman and Amson.[11,12] We inoculated a culture of human RPMI8226 myeloma cells, derived from a single clone by limiting dilution, with the H-1 virus. This treatment caused the progressive degeneration of the culture. Maintenance of this culture led to further degeneration of the myeloma cells, leaving a single clone that was recovered 3 months after infection. This clone (named hereafter RPMI8226-RC) was expanded into a continuously growing cell line. The rescued clone is thus resistant to the cytopathic effect of the H-1 virus.

Using PCR analysis, we detected viral DNA in RPMI8226-RC cells 3 months after infection (Figure 1A). However, adding supernatant from the RPMI8226-RC culture to the original uninfected RPMI8226 cells did not give rise to a cytopathic effect, indicating that revertant cells do not produce virus anymore (data not shown). These results suggested that persistent infection and expression of the H1 parvovirus is not necessary for maintaining the suppressed malignant phenotype in the MM revertant cells.

To exclude contamination of the parental RPMI8226 cell population with other cells and to confirm the genetic lineage of the RPMI8226-RC cell line as a derivative of the parental RPMI8226 myeloma cell line, we compared the DNA fingerprinting pattern of RPMI8226 cells with that of revertant cells using nine different genetic markers (8 STR markers and the Amelogenin locus). The RPMI8226 cell line and revertant RPMI8226-RC cells had identical DNA fingerprinting patterns for all genetic markers (Table 1). Thus, STR analyses confirmed that revertant cells were derived from RPMI8226 cells and were not a result of cross-contamination.

Analysis of MM Revertant Cells. Revertant cells retained many of the properties of parental MM cells. Table 2 summarizes the growth properties of RPMI8226 and RPMI8226-RC cells. Under standard culture conditions, both cell lines had a comparable growth pattern with a population doubling time of around 40 h, similar proportions of cells in the G1, S, and G2 plus M phases, and a similar apoptotic ratio.

However, there were many differences between the two cell lines with regard to their transformed and tumorigenic properties. As shown in Table 2, colony-forming efficiency was significantly lower for revertant cells in soft agar. The hallmark of terminally differentiated normal and malignant B cells is production and secretion of immunoglobulins. RPMI 8226 characteristically produces λ free light chains (FLC).[38] Thus, we tested the secretion of λ FLCs in both cell lines and found a significant decrease in secreted λ FLCs in revertant cells (Table 2). We further investigated if the reduction in secreted levels of λ FLCs in revertant cells was due to secretion inhibition or to a block in differentiation. To this end, cytoplasmic Ig (λ)

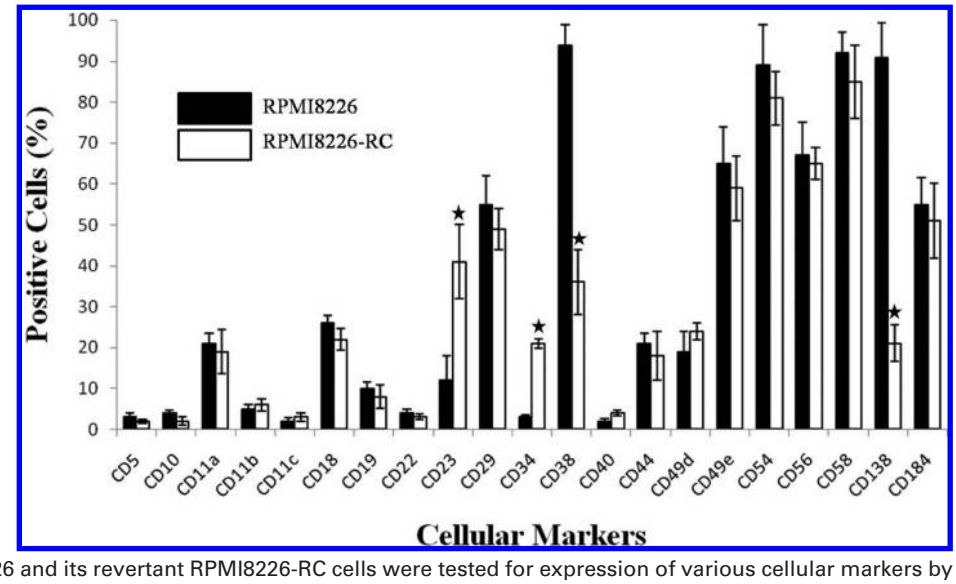

Figure 2. RPMI 8226 and its revertant RPMI8226-RC cells were tested for expression of various cellular markers by flow cytometry. The means ± SD (bars) of three independent experiments are shown. * $P < 0.05$.

staining was performed; both the number and the intensity of cIg (λ) positive cells were negatively affected in revertant cells (Figure 1B).

These phenotypic changes in revertant cells may relate to a shift in MM differentiation. Thus, we further evaluated the differential expression of various cellular markers in both cell lines. As shown in Figure 2, of the cellular markers examined, CD5, CD10, CD11b, CD11c, CD19, CD22, and CD40 molecules were barely detectable in both cell lines, while CD11a, CD18, CD44, and CD49d were expressed at low levels in both cell lines. CD29, CD49e, CD54, CD56, CD58, and CD184 were expressed highly in both RPMI8226 and RPMI8226-RC cells. In contrast, RPMI8226-RC cells displayed a significant increase in the percentage of CD23 and CD34 positive cells and a decrease in the percentage of CD38 and CD138 positive cells.

In vivo tumorigenicity of RPMI8226-RC and parental RPMI8226 cells was tested in nod/scid mice and was found to be much lower for RPMI8226-RC cells than for parental cells (Figure 1C). RPMI8226-RC formed four tumors after 20 injections, whereas parental RPMI8226 cells formed 19 tumors. The size of the tumors was also significantly lower when revertant cells were injected ($p < 0.05$).

Collectively, our results suggest that RPMI8226-RC cells show partial phenotypic reversion of terminally differentiated B tumor cells and a suppressed malignant phenotype.

Quantitative Proteome Analysis of Myeloma Reversion. To investigate this difference in tumorigenicity and phenotype at the molecular level, we compared the overall expression of proteins using the SILAC method. The workflow in this study is outlined in Figure 3A. According to the criteria described in the Experimental Procedures, 20 of the 2050 quantified proteins were up-regulated 2.0-fold or greater, and 359 were down regulated 2.0-fold or greater in RPMI8226-RC cells. Table S1 (Supporting Information) lists the differentially expressed proteins and their molecular functions. A list of all quantified proteins is shown in Table S2 (Supporting Information). These DEPs provide a global view of the protein variation that occurs during the process of myeloma reversion.

To further confirm the SILAC ratios observed with MS, we used Western blotting to examine the expression of a selected panel of proteins, including SRP54, H2AFX, HSPA1A, PSMC5, EIF5, S100A11, PLK1, YWHAQ, STAT3, TCTP/*tpt1*, STAT5A, BAG2, PCNA, CDC2, VIM, and HSPB1. As shown in Figure 3B, the Western blotting results for all the selected proteins showed the same pattern of expression as that obtained from SILAC experiments.

Functional Categories and an Association Network of Identified Proteins. To understand the biological relevance of the changes in protein expression in revertant cells, the PANTHER classification system was used; the 379 identified DEPs were classified into 26 groups according to their molecular functions (Figure 4A). These proteins are implicated in a broad range of cellular activities. Proteins involved in nucleic acid binding account for the largest portion (33%). There are also a significant number of proteins involved in cytoskeletal, regulatory molecule, and kinase activities.

Table S1 (Supporting Information) simply provides a list of DEPs in RPMI8226-RC cells but lacks information on their biochemical contexts. To create significance out of otherwise static proteomic data, we constructed a biological interaction network for the DEPs (Figure 4B). DEPs that could be networked were linked by various relationships such as protein interactions, modifications, and regulation of expression. Table S3 (Supporting Information) provides information on the proteins and the nature of their interactions with each other. This should be useful for formulating testable hypotheses to understand the function of the identified DEPs in RPMI8226-RC cells. The protein with the greatest number of connections was STAT3 (329 connections); this protein represents a central node in the mapped DEPs (Figure 4B).

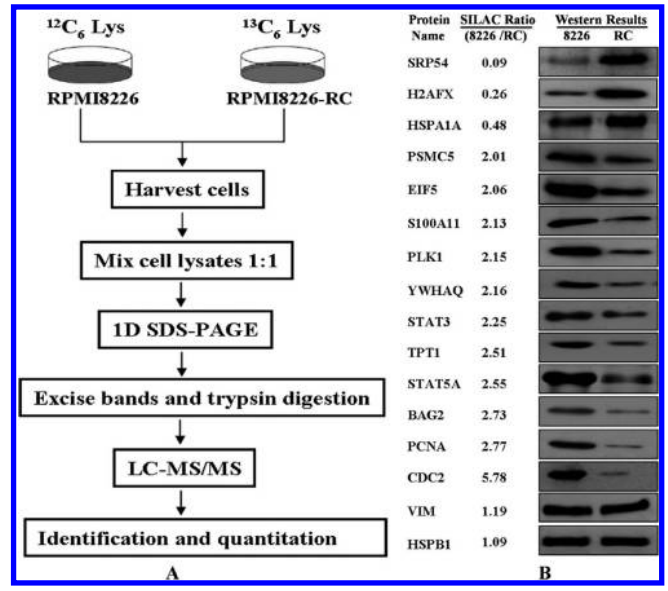

Figure 3. Quantitative proteome analysis of MM reversion. (A) Schematic showing application of SILAC for differential proteomic profiling of MM reversion. The parental RPMI8226 cells and revertant RPMI8226-RC cells were grown in RPMI1640 containing light ($^{12}C_6$) or heavy ($^{13}C_6$) lysine, respectively. Equal amounts of protein from RPMI8226-RC (^{13}C6-lysine) and parental RPMI8226 ($^{12}C_6$-lysine) cells were mixed at a 1:1 ratio and separated by SDS-PAGE. The gel lane was cut into 30 bands, digested in-gel with trypsin, and analyzed by LC−MS/MS for protein identification and quantification. Each peptide was quantified by measuring the peak area of light and heavy peptides in the MS spectra using CENSUS. (B) Western blot images for 14 differentially expressed proteins and the internal control proteins VIM and HSPB1. The pattern of expression of all the selected proteins detected by Western blotting results was the same as that obtained from SILAC experiments. 8226, parental RPMI8226 cells; RC, RPMI8226-RC cells.

Myeloma Reversion Operates, at Least in Part, Through Inhibition of STAT3. To investigate whether STAT3 has a role in cell growth control and tumorigenesis and to explore the consequence of STAT3 inhibition, we used RNAi to reduce cellular STAT3 levels. Two stable RPMI8226 cell lines were established expressing distinct shRNA that targets STAT3 mRNA, termed MM-KD1 and KD2. Using quantitative real-time polymerase chain reactions (PCRs), two clones (MM-KD1 and KD2) showed a dramatic reduction in STAT3 mRNA compared to parental control cells or transfected control cells. The two clones with shRNA against STAT3 showed a greater than 50% reduction in STAT3 mRNA (Figure 5A). Immunoblot analysis demonstrated a reduction in the expression level of STAT3 protein in these two clones (Figure 5B). We next studied whether myeloma reversion interferes with the activation of STAT3, that is, with the phosphorylation of tyrosine residue 705. RPMI 8226 cells do not express constitutively phosphorylated STAT3, and phosphorylation of STAT3 is induced by IL-6 treatment.[40,41] Therefore, to examine the status of STAT3

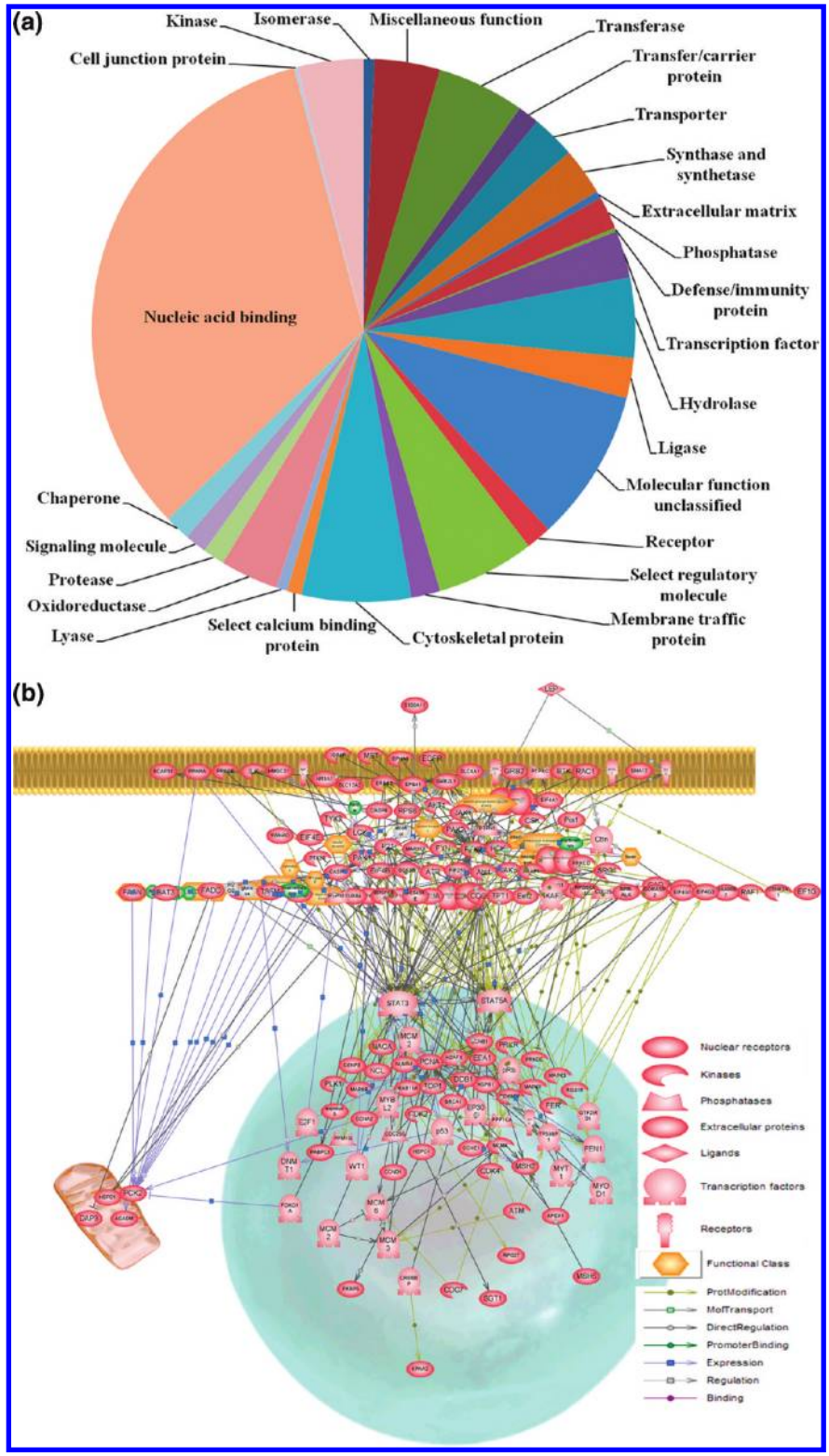

Figure 4. Bioinformatic analysis of identified DEPs. (A) Pie chart representation of the distribution of identified DEPs according to their molecular functions. Categorization was based on the PANTHER classification system. (B) Pathway mapping of DEPs was carried out using Pathway Studio. Identified DEPs listed in Table S1 (Supporting Information) were imported into PathwayAssist, and an interaction map was generated. Each node represents either a protein entity or a control mechanism of the interaction. The legend of the interaction network is summarized on the right of the figure.

phosphorylation, RPMI 8226 cells were treated with or without IL-6 (10 ng/mL) for 30 min. As shown in Figure 6, IL-6 can induce STAT3 phosphorylation in RPMI8226 cells. Compared with parental PRMI8226 and MM-NC cells, the expression of STAT3 and phospho-STAT3 (pY705) proteins decreased significantly in PRMI8226-RC, MM-KD1, and MM-KD2 cells. Results show that myeloma reversion inhibits constitutive expression and activation of STAT3.

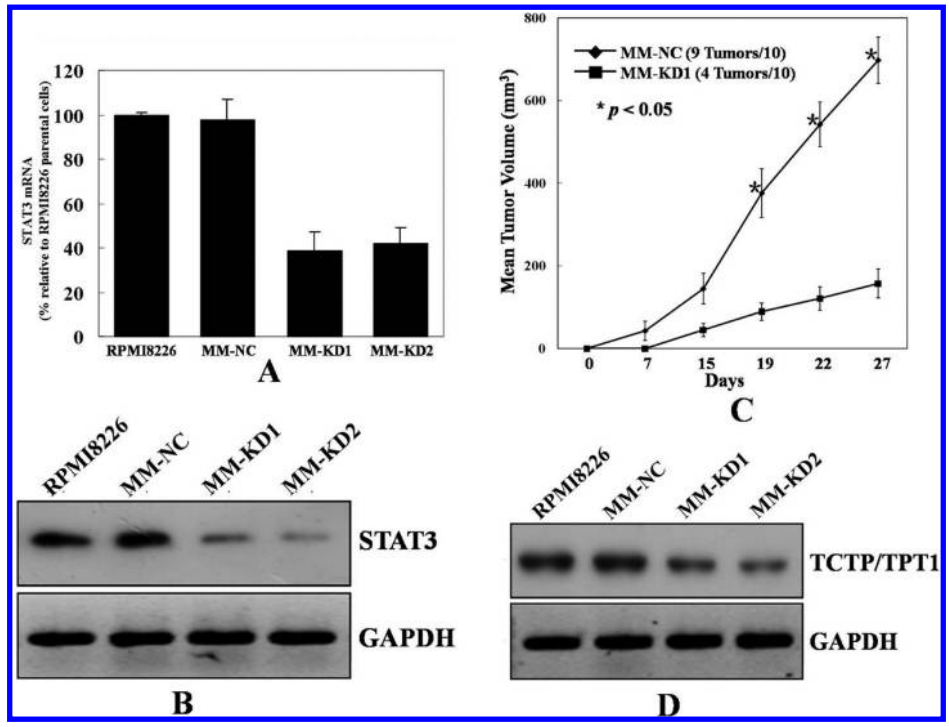

Figure 5. Inhibition of STAT3 expression led to suppression of the malignant phenotype in MM cells. MM-NC, RPMI8226 cells stably transfected with pSiStrike/control; MM-KD1 or KD2, RPMI8226 cells stably transfected with pSiStrike/STAT3. (A) Quantification of mRNA revealed markedly reduced mRNA in MM-KD1 and KD2 cells compared to parental RPMI8226 cells or cells transfected with control vector (MM-NC). Quantitative PCR was performed as described in the Experimental Procedures section. Means and standard errors are shown. (B) Suppression of STAT3 in RPMI8226 cells was confirmed by Western blotting. (C) STAT3 suppression led to suppressed in vivo tumorigenicity. (D) Western blots showing that suppression of STAT3 decreases the level of TCTP/*tpt1*.

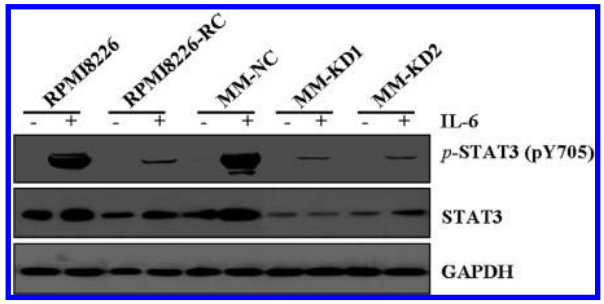

Figure 6. Expression of STAT3 and phospho-STAT3 (pY705) proteins was decreased significantly in PRMI8226-RC, MM-KD1, and MM-KD2 cells. Cells were treated with (+) or without (−) IL-6 (10 ng/mL) for 30 min, and whole-cell extracts were prepared. An amount of 30 μg of whole cell extracts was resolved on 10% SDS-PAGE, electrotransferred to a nitrocellulose membrane, and probed for the pY705 (upper panel), STAT3 (middle panel), and GAPDH (lower panel). Results shown are for one representative experiment of three.

As shown in Table 3, suppression of STAT3 led to a significant decrease in the proliferation of RPMI8226 cells compared with control cells. This decrease in STAT3 also led to an increased rate of apoptosis (Table 3). To determine whether this growth inhibition was associated with specific changes in cell cycle distribution, cell cycle analysis was carried out in MM-KD and MM-NC cells. The data shown in Table 3 indicate that MM-KD cells accumulate significantly in the G1 phase compared with the control.

Soft agar colony assays showed that MM-KD1 and MM-KD2 cells had markedly lower colony forming abilities (Table 3). When MM-KD1 cells were injected into NOD/SCID mice, they showed a robust inhibition of tumorigenicity (Figure 5C). After four weeks of injections of cells, MM-KD1 cells formed four tumors; however, the negative control MM-NC cells formed tumors in 90% of the injections, and the size of the tumors in MM-KD1 was significantly lower ($p < 0.05$). These data indicate that STAT3 suppression can significantly decrease tumor growth in vivo. Since TCTP/*tpt1* has been reported to be a gene that is down regulated in tumor reversion and since down regulation of TCTP/*tpt1* can induce tumor reversion,[11] we investigated the impact of the STAT3 knock-down on TCTP/*tpt1* expression. As shown in Figure 5D, TCTP/*tpt1* expression was reduced in MM-KD1 and MM-KD2 cells. Overall, our results suggest that STAT3 may act upstream of TCTP/*tpt1* and that myeloma reversion operates, at least in part, through inhibition of STAT3.

Table 3. Summary of the Growth Properties of RPMI8226, Negative Control (MM-NC), and STAT3 Knock-Down Cells (MM-KD1 and KD2)

	RPMI1640/10% FBS		soft agar	annexin V/PI staining
cell	doubling time (h)	G1/S/G2/M phase, %	CFE (%)	apoptotic ratio (%)
RPMI8226	36	58/28/14	24 ± 2.2	2.3 ± 1.1
MM-NC	37	56/29/15	22 ± 3.1	2.8 ± 0.8
MM-KD1	65	70/18/12	7.3 ± 1.8	16.2 ± 2.2
MM-KD2	62	68/19/13	5.8 ± 2.7	14.3 ± 3.1

Discussion

In previous reports, Telerman and Amson used the H1 parvovirus as a selective agent to derive biological models of tumor reversion from different tumor cell lines, including the erythroleukemia cell line K562, the myelomonocytic leukemia cell line U937, and three major solid cancer cell lines.[11,12]

Hendrix's group demonstrated the reversion of the metastatic phenotype of aggressive melanoma cells by using an embryonic microenvironment.[39,40] These models provided novel insights into the mechanisms of tumor reversion and may contribute to the development of novel therapeutic strategies. We initiated our work by asking whether terminally differentiated tumor-derived B cells, namely, multiple myeloma (MM) cells, have the capacity to revert. For the first time, using the same methodology as Telerman and Amson,[7−12] we derived revertants from MM cells and established a biological model of multiple myeloma tumor reversion. As demonstrated here, these MM revertant cells have a strongly suppressed malignant phenotype both in vitro and in vivo.

An interesting aspect of our results is that reversion of these terminally differentiated cells can down regulate the typically plasmacytoid markers CD38 and CD138 and reduce λ light chain production and secretion. Furthermore, revertant cells gained expression of CD23, a B-cell marker, and CD34, a hematopoietic stem cell marker. Under normal B cell differentiation circumstances, the plasma cell program is irreversible, and committed plasma cells never revert to B cells in vivo.[41] However, a line of evidence is emerging that myeloma cells have the ability to reprogram, dedifferentiate, and acquire autonomous survival properties. It has been shown that some mouse $CD45^-$ 5T multiple myeloma cells can re-express CD45[42] and that murine $CD45^+$ multiple myeloma cells are quiescent, slowly proliferative, and resistant to drug-induced apoptosis, but highly invasive.[43,44] Yaccoby further demonstrated that myeloma cells have the ability to reprogram and dedifferentiate into an immature, resilient phenotype and become autonomous after coculture with osteoclasts.[45] Recently, Anastasiadou et al. showed that Epstein−Barr virus infection leads to partial phenotypic reversion in MM cells.[46] Consistent with these reports, our data suggest that the H1 parvovirus can select phenotypic revertants of MM cells. The current study suggests that there is an alternative pathway or mechanism inhibited in MM cells that, if triggered, would enable MM cells to exit the malignant pathway by adopting a less differentiated phenotype.

To gain insight into the molecular events that are important for MM reversion, we compared the protein profiles of the revertant cells and parental MM cells using a quantitative proteomic strategy. Our results revealed that 379 of the 2050 quantified proteins had significantly altered levels of expression (Tables S1 and S2, Supporting Information). These proteins can be categorized into up- and down-regulated groups according to their expression patterns (Table S1, Supporting Information). Notably, the vast majority of the proteins was down regulated during reversion (359 versus 20 which were up-regulated). This unbalanced expression pattern is consistent with previous results from comparative microarray profiling of normal plasma cells (NPC) and MM cells.[47] Zhan and colleagues have shown that more than 90% of differentially expressed genes exhibited an increase in expression level with the transition from NPC to MGUS to MM.[47] MM cells are characterized by the overproduction of monoclonal immunoglobulins and activation of multiple growth and survival pathways. We therefore speculate that MM cells may revert their malignant phenotype by down regulation of promiscuous gene expression and by the normalization of signal transduction pathways. It is noteworthy that 195 nucleic acid binding proteins were dysregulated in their expression (Figure 4A). Thus, the dysregulation of these specific proteins may constitute one of the mechanisms of myeloma reversion. The PANTHER classification system also revealed that DEPs were implicated in a variety of functional groups, such as cytoskeletal proteins, regulatory molecules, and kinases (Figure 4A), exemplifying the multiple layers of coordinated molecular control in the process of myeloma reversion. However, these changes may equally be a consequence of the reversion process and not necessarily contribute to it. Further functional studies will be needed before cause−effect conclusions can be drawn.

Interestingly, translationally controlled tumor protein 1 (TCTP/*tpt1*) was significantly down regulated in revertant cells, and its alteration was further confirmed by Western blotting. TCTP/*tpt1* was discovered in Ehrlich ascite tumor cells[48] and characterized as a histamine-releasing factor.[49−51] TCTP/*tpt1* has been shown to regulate the cytoskeleton[52,53] and protein synthesis[22] and inhibit apoptosis.[11,12,20,54−57] Our findings are consistent with previous studies which have demonstrated that down regulation of TCTP/*tpt1* can induce tumor reversion.[11] Other studies have identified some pharmacological compounds which can decrease the level of TCTP/*tpt1* and kill tumor cells.[12] Therefore, we deduced that down regulation of TCTP/*tpt1* could be one of the mechanisms of myeloma reversion.

Notably, bioinformatic analysis revealed that the protein with the greatest number of connections was STAT3, suggesting that the STAT pathway may play a central role in the process of myeloma reversion. STAT is a family of transcription factors that has been associated with the inflammation, survival, proliferation, metastasis, angiogenesis, and chemoresistance of tumor cells.[58] One member of this family, namely, STAT3, is constitutively expressed in multiple myeloma (MM), leukemia, lymphoma, squamous cell carcinoma, and other solid tumors, including cancers of the prostate, breast, head and neck, and nasopharynx.[59,60] STAT3 plays a crucial role in hematopoiesis, in mediating immune responses, and in the regulation of differentiation.[61] STAT3 target genes have been identified and include regulators of crucial steps in oncogenesis.[62,63] Molecular targeting of STAT3 in preclinical models of human cancer using a variety of strategies has been shown to cause the suppression of tumor cell growth and the induction of apoptosis.[64,65] On the basis of the critical role of STAT3 in tumor cell survival, proliferation, and angiogenesis, we hypothesized that myeloma reversion operates, at least in part, through suppression of the STAT3 pathway. Data presented here indicate that inhibition of STAT3 expression by RNA interference leads to induced cell apoptosis, decreased cell proliferation, and suppression of the malignant phenotype both in vitro and in vivo. Furthermore, our results demonstrate that both myeloma reversion and STAT3 knock-down can inhibit constitutive expression of STAT3 in MM cells (Figure 6). By investigating the impact of STAT3 knock-down on TCTP/*tpt1* expression, we showed that inhibition of STAT3 results in down regulation of TCTP/*tpt1*. This indicates that STAT3 can be placed in this network as acting upstream of TCTP/*tpt1*. We suggest that reversion as described here operates through at least three mechanisms. The first mechanism involves the inhibition of the expression of hundreds of nucleic acid binding proteins listed in Table S1 (Supporting Information). The second mechanism is by inhibiting expression of TCTP/*tpt1* as previously reported.[11,12,20−22] The third mechanism involves the STAT3 pathway, as described in this study. The combination of all three mechanisms may reprogram the MM cell to recover some of its normal functions. However, as shown in

Tables 2 and 3, there are some phenotypic differences between revertant and STAT3 knock-down cells with regard to their growth properties and levels of apoptosis. Thus, it is possible that the complexity of the process may be much greater than presently envisaged and that other proteins described in Table S1 (Supporting Information) may be as important as STAT3 or TCTP/*tpt1* in controlling reversion.

In conclusion, we have developed the first biological model for studying MM reversion by using the H-1 parvovirus as a tool[7−12] to isolate revertants among millions of MM cells. The quantitative proteomics analysis described here identified many proteins that potentially affect MM reversion and implicate previously unconsidered pathways in the process of tumor reversion. By using siRNA, we also obtained evidence that depletion of STAT3 results in suppression of the malignant phenotype. Our findings provide some molecular explanations for tumor reversion in MM and could lead to the development of new anticancer drugs.

Abbreviations: MM, multiple myeloma; SILAC, stable isotope labeling by amino acids in cell culture; STAT3, signal transducer and activator of transcription 3; TCTP, translationally controlled tumor protein; DEPs, differentially expressed proteins; CFE, colony-forming efficiency; FBS, fetal bovine serum; FLC, free light chain; PANTHER, protein analysis through evolutionary relationships; STR, short tandem repeat.

Acknowledgment. This work was supported by the Hundred Talents Program of the Chinese Academy of Sciences, the National Protein Research Fund (Grant No: 2009CB825400 and 2006CB910902), the Infectious Diseases Control Project of the Ministry of Health of China (No. 2009ZX10004-107), the Major Special Program on Infectious Diseases of the Ministry of Health of China (2008ZX10003-005), the State Key Development Program for Basic Research of China (Grant No. 2010CB529205), the Program for New Century Excellent Talents in University (NCET-09-551), and a Grant-in-Aid for Scientific Research from the Japan Society for the Promotion of Science (JSPS).

Supporting Information Available: Tables S1−S3. This material is available free of charge via the Internet at http://pubs.acs.org.

References

(1) Mitsiades, C. S.; Mitsiades, N.; Munshi, N. C.; Anderson, K. C. Focus on multiple myeloma. *Cancer Cell* **2004**, *6* (5), 439–44.
(2) Kyle, R. A.; Rajkumar, S. V. Monoclonal gammopathy of undetermined significance. *Br. J. Haematol.* **2006**, *134* (6), 573–89.
(3) Jemal, A.; Siegel, R.; Ward, E.; Hao, Y.; Xu, J.; Murray, T.; Thun, M. J. Cancer statistics, 2008. *CA Cancer J. Clin.* **2008**, *58* (2), 71–96.
(4) Barlogie, B.; Shaughnessy, J.; Tricot, G.; Jacobson, J.; Zangari, M.; Anaissie, E.; Walker, R.; Crowley, J. Treatment of multiple myeloma. *Blood* **2004**, *103* (1), 20–32.
(5) Tassone, P.; Tagliaferri, P.; Rossi, M.; Gaspari, M.; Terracciano, R.; Venuta, S. Genetics and molecular profiling of multiple myeloma: novel tools for clinical management. *Eur. J. Cancer* **2006**, *42* (11), 1530–8.
(6) Hideshima, T.; Mitsiades, C.; Tonon, G.; Richardson, P. G.; Anderson, K. C. Understanding multiple myeloma pathogenesis in the bone marrow to identify new therapeutic targets. *Nat. Rev. Cancer* **2007**, *7* (8), 585–98.
(7) Telerman, A.; Amson, R. The molecular programme of tumour reversion: the steps beyond malignant transformation. *Nat. Rev. Cancer* **2009**, *9* (3), 206–16.
(8) Telerman, A.; Tuynder, M.; Dupressoir, T.; Robaye, B.; Sigaux, F.; Shaulian, E.; Oren, M.; Rommelaere, J.; Amson, R. A model for tumor suppression using H-1 parvovirus. *Proc. Natl. Acad. Sci. U.S.A.* **1993**, *90* (18), 8702–6.
(9) Nemani, M.; Linares-Cruz, G.; Bruzzoni-Giovanelli, H.; Roperch, J. P.; Tuynder, M.; Bougueleret, L.; Cherif, D.; Medhioub, M.; Pasturaud, P.; Alvaro, V.; der Sarkissan, H.; Cazes, L.; Le Paslier, D.; Le Gall, I.; Israeli, D.; Dausset, J.; Sigaux, F.; Chumakov, I.; Oren, M.; Calvo, F.; Amson, R. B.; Cohen, D.; Telerman, A. Activation of the human homologue of the Drosophila sina gene in apoptosis and tumor suppression. *Proc. Natl. Acad. Sci. U.S.A.* **1996**, *93* (17), 9039–42.
(10) Linares-Cruz, G.; Bruzzoni-Giovanelli, H.; Alvaro, V.; Roperch, J. P.; Tuynder, M.; Schoevaert, D.; Nemani, M.; Prieur, S.; Lethrosne, F.; Piouffre, L.; Reclar, V.; Faille, A.; Chassoux, D.; Dausset, J.; Amson, R. B.; Calvo, F.; Telerman, A. p21WAF-1 reorganizes the nucleus in tumor suppression. *Proc. Natl. Acad. Sci. U.S.A.* **1998**, *95* (3), 1131–5.
(11) Tuynder, M.; Susini, L.; Prieur, S.; Besse, S.; Fiucci, G.; Amson, R.; Telerman, A. Biological models and genes of tumor reversion: cellular reprogramming through tpt1/TCTP and SIAH-1. *Proc. Natl. Acad. Sci. U.S.A.* **2002**, *99* (23), 14976–81.
(12) Tuynder, M.; Fiucci, G.; Prieur, S.; Lespagnol, A.; Geant, A.; Beaucourt, S.; Duflaut, D.; Besse, S.; Susini, L.; Cavarelli, J.; Moras, D.; Amson, R.; Telerman, A. Translationally controlled tumor protein is a target of tumor reversion. *Proc. Natl. Acad. Sci. U.S.A.* **2004**, *101* (43), 15364–9.
(13) Braun, A. C. Recovery of tumor cells from effects of the tumor-inducing principle in crown gall. *Science* **1951**, *113* (2945), 651–3.
(14) Braun, A. C. A Demonstration of the Recovery of the Crown-Gall Tumor Cell with the Use of Complex Tumors of Single-Cell Origin. *Proc. Natl. Acad. Sci. U.S.A.* **1959**, *45* (7), 932–8.
(15) Pierce, G. B.; Dixon, F. J., Jr. Testicular teratomas. I. Demonstration of teratogenesis by metamorphosis of multipotential cells. *Cancer* **1959**, *12* (3), 573–83.
(16) Seilern-Aspang, F.; Kratochwil, K. Induction and differentiation of an epithelial tumour in the newt (Triturus cristatus). *J. Embryol. Exp. Morphol.* **1962**, *10*, 337–56.
(17) Noda, M.; Kitayama, H.; Matsuzaki, T.; Sugimoto, Y.; Okayama, H.; Bassin, R. H.; Ikawa, Y. Detection of genes with a potential for suppressing the transformed phenotype associated with activated ras genes. *Proc. Natl. Acad. Sci. U.S.A.* **1989**, *86* (1), 162–6.
(18) Kitayama, H.; Sugimoto, Y.; Matsuzaki, T.; Ikawa, Y.; Noda, M. A ras-related gene with transformation suppressor activity. *Cell* **1989**, *56* (1), 77–84.
(19) Ryuya, M.; Teruyuki, M.; Emi, N.; Yoko, M.; Hitoshi, K.; Shinae, K.; Yoshinori, K.; Masahiro, H.; Motonari, U.; Makoto, N. A novel screen using the Reck tumor suppressor gene promoter detects both conventional and metastasis-suppressing anticancer drugs. *Oncotarget* **2010**, *1* (4), 12.
(20) Susini, L.; Besse, S.; Duflaut, D.; Lespagnol, A.; Beekman, C.; Fiucci, G.; Atkinson, A. R.; Busso, D.; Poussin, P.; Marine, J. C.; Martinou, J. C.; Cavarelli, J.; Moras, D.; Amson, R.; Telerman, A. TCTP protects from apoptotic cell death by antagonizing bax function. *Cell Death Differ.* **2008**, *15* (8), 1211–20.
(21) Lespagnol, A.; Duflaut, D.; Beekman, C.; Blanc, L.; Fiucci, G.; Marine, J. C.; Vidal, M.; Amson, R.; Telerman, A. Exosome secretion, including the DNA damage-induced p53-dependent secretory pathway, is severely compromised in TSAP6/Steap3-null mice. *Cell Death Differ.* **2008**, *15* (11), 1723–33.
(22) Cans, C.; Passer, B. J.; Shalak, V.; Nancy-Portebois, V.; Crible, V.; Amzallag, N.; Allanic, D.; Tufino, R.; Argentini, M.; Moras, D.; Fiucci, G.; Goud, B.; Mirande, M.; Amson, R.; Telerman, A. Translationally controlled tumor protein acts as a guanine nucleotide dissociation inhibitor on the translation elongation factor eEF1A. *Proc. Natl. Acad. Sci. U.S.A.* **2003**, *100* (24), 13892–7.
(23) Ong, S. E.; Blagoev, B.; Kratchmarova, I.; Kristensen, D. B.; Steen, H.; Pandey, A.; Mann, M. Stable isotope labeling by amino acids in cell culture, SILAC, as a simple and accurate approach to expression proteomics. *Mol. Cell. Proteomics* **2002**, *1* (5), 376–86.
(24) Chen, N.; Sun, W.; Deng, X.; Hao, Y.; Chen, X.; Xing, B.; Jia, W.; Ma, J.; Wei, H.; Zhu, Y.; Qian, X.; Jiang, Y.; He, F. Quantitative proteome analysis of HCC cell lines with different metastatic potentials by SILAC. *Proteomics* **2008**, *8* (23−24), 5108–18.
(25) Sun, Y.; Mi, W.; Cai, J.; Ying, W.; Liu, F.; Lu, H.; Qiao, Y.; Jia, W.; Bi, X.; Lu, N.; Liu, S.; Qian, X.; Zhao, X. Quantitative proteomic signature of liver cancer cells: tissue transglutaminase 2 could be a novel protein candidate of human hepatocellular carcinoma. *J. Proteome Res.* **2008**, *7* (9), 3847–59.
(26) Kratchmarova, I.; Blagoev, B.; Haack-Sorensen, M.; Kassem, M.; Mann, M. Mechanism of divergent growth factor effects in mesenchymal stem cell differentiation. *Science* **2005**, *308* (5727), 1472–7.

(27) Blagoev, B.; Ong, S. E.; Kratchmarova, I.; Mann, M. Temporal analysis of phosphotyrosine-dependent signaling networks by quantitative proteomics. *Nat. Biotechnol.* **2004**, *22* (9), 1139–45.
(28) Zhang, L.; Zhang, Z. P.; Zhang, X. E.; Lin, F. S.; Ge, F. Quantitative proteomics analysis reveals BAG3 as a potential target to suppress severe acute respiratory syndrome coronavirus replication. *J. Virol.* **2010**, *84* (12), 6050–9.
(29) Ge, F.; Lu, X. P.; Zeng, H. L.; He, Q. Y.; Xiong, S.; Jin, L.; He, Q. Y. Proteomic and functional analyses reveal a dual molecular mechanism underlying arsenic-induced apoptosis in human multiple myeloma cells. *J. Proteome Res.* **2009**, *8* (6), 3006–19.
(30) St-Germain, J. R.; Taylor, P.; Tong, J.; Jin, L. L.; Nikolic, A.; Stewart, I. I.; Ewing, R. M.; Dharsee, M.; Li, Z.; Trudel, S.; Moran, M. F. Multiple myeloma phosphotyrosine proteomic profile associated with FGFR3 expression, ligand activation, and drug inhibition. *Proc. Natl. Acad. Sci. U.S.A.* **2009**, *106* (47), 20127–32.
(31) Rees-Unwin, K. S.; Craven, R. A.; Davenport, E.; Hanrahan, S.; Totty, N. F.; Dring, A. M.; Banks, R. E.; G, J. M.; Davies, F. E. Proteomic evaluation of pathways associated with dexamethasone-mediated apoptosis and resistance in multiple myeloma. *Br. J. Haematol.* **2007**, *139* (4), 559–67.
(32) Chen, Y. Q.; de Foresta, F.; Hertoghs, J.; Avalosse, B. L.; Cornelis, J. J.; Rommelaere, J. Selective killing of simian virus 40-transformed human fibroblasts by parvovirus H-1. *Cancer Res.* **1986**, *46* (7), 3574–9.
(33) Dagvadorj, A.; Tan, S. H.; Liao, Z.; Cavalli, L. R.; Haddad, B. R.; Nevalainen, M. T. Androgen-regulated and highly tumorigenic human prostate cancer cell line established from a transplantable primary CWR22 tumor. *Clin. Cancer Res.* **2008**, *14* (19), 6062–72.
(34) Park, S. K.; Venable, J. D.; Xu, T.; Yates, J. R., III. A quantitative analysis software tool for mass spectrometry-based proteomics. *Nat. Methods* **2008**, *5* (4), 319–22.
(35) Mi, H.; Guo, N.; Kejariwal, A.; Thomas, P. D. PANTHER version 6: protein sequence and function evolution data with expanded representation of biological pathways. *Nucleic Acids Res.* **2007**, *35* (Database issue), D247–52.
(36) Nikitin, A.; Egorov, S.; Daraselia, N.; Mazo, I. Pathway studio--the analysis and navigation of molecular networks. *Bioinformatics* **2003**, *19* (16), 2155–7.
(37) Chatterjee, M.; Stuhmer, T.; Herrmann, P.; Bommert, K.; Dorken, B.; Bargou, R. C. Combined disruption of both the MEK/ERK and the IL-6R/STAT3 pathways is required to induce apoptosis of multiple myeloma cells in the presence of bone marrow stromal cells. *Blood* **2004**, *104* (12), 3712–21.
(38) Matsuoka, Y.; Moore, G. E.; Yagi, Y.; Pressman, D. Production of free light chains of immunoglobulin by a hematopoietic cell line derived from a patient with multiple myeloma. *Proc. Soc. Exp. Biol. Med.* **1967**, *125* (4), 1246–50.
(39) Hendrix, M. J.; Seftor, E. A.; Seftor, R. E.; Kasemeier-Kulesa, J.; Kulesa, P. M.; Postovit, L. M. Reprogramming metastatic tumour cells with embryonic microenvironments. *Nat. Rev. Cancer* **2007**, *7* (4), 246–55.
(40) Kulesa, P. M.; Kasemeier-Kulesa, J. C.; Teddy, J. M.; Margaryan, N. V.; Seftor, E. A.; Seftor, R. E.; Hendrix, M. J. Reprogramming metastatic melanoma cells to assume a neural crest cell-like phenotype in an embryonic microenvironment. *Proc. Natl. Acad. Sci. U.S.A.* **2006**, *103* (10), 3752–7.
(41) Shapiro-Shelef, M.; Calame, K. Regulation of plasma-cell development. *Nat. Rev. Immunol.* **2005**, *5* (3), 230–42.
(42) Asosingh, K.; De Raeve, H.; Croucher, P.; Goes, E.; Van Riet, I.; Van Camp, B.; Vanderkerken, K. In vivo homing and differentiation characteristics of mature (CD45-) and immature (CD45+) 5T multiple myeloma cells. *Exp. Hematol.* **2001**, *29* (1), 77–84.
(43) Asosingh, K.; Willems, A.; Van Riet, I.; Van Camp, B.; Vanderkerken, K. Delayed in vivo disease progression is associated with high proportions of CD45+ myeloma cells in the 5T2MM murine model. *Cancer Res.* **2003**, *63* (12), 3019–20.
(44) Vanderkerken, K.; Asosingh, K.; Croucher, P.; Van Camp, B. Multiple myeloma biology: lessons from the 5TMM models. *Immunol. Rev.* **2003**, *194*, 196–206.
(45) Yaccoby, S. The phenotypic plasticity of myeloma plasma cells as expressed by dedifferentiation into an immature, resilient, and apoptosis-resistant phenotype. *Clin. Cancer Res.* **2005**, *11* (21), 7599–606.
(46) Anastasiadou, E.; Vaeth, S.; Cuomo, L.; Boccellato, F.; Vincenti, S.; Cirone, M.; Presutti, C.; Junker, S.; Winberg, G.; Frati, L.; Wade, P. A.; Faggioni, A.; Trivedi, P. Epstein-Barr virus infection leads to partial phenotypic reversion of terminally differentiated malignant B cells. *Cancer Lett.* **2009**, *284* (2), 165–74.
(47) Zhan, F.; Barlogie, B.; Arzoumanian, V.; Huang, Y.; Williams, D. R.; Hollmig, K.; Pineda-Roman, M.; Tricot, G.; van Rhee, F.; Zangari, M.; Dhodapkar, M.; Shaughnessy, J. D., Jr. Gene-expression signature of benign monoclonal gammopathy evident in multiple myeloma is linked to good prognosis. *Blood* **2007**, *109* (4), 1692–700.
(48) Yenofsky, R.; Bergmann, I.; Brawerman, G. Messenger RNA species partially in a repressed state in mouse sarcoma ascites cells. *Proc. Natl. Acad. Sci. U.S.A.* **1982**, *79* (19), 5876–80.
(49) MacDonald, S. M.; Rafnar, T.; Langdon, J.; Lichtenstein, L. M. Molecular identification of an IgE-dependent histamine-releasing factor. *Science* **1995**, *269* (5224), 688–90.
(50) Schroeder, J. T.; Lichtenstein, L. M.; MacDonald, S. M. Recombinant histamine-releasing factor enhances IgE-dependent IL-4 and IL-13 secretion by human basophils. *J. Immunol.* **1997**, *159* (1), 447–52.
(51) Vonakis, B. M.; Macglashan, D. W., Jr.; Vilarino, N.; Langdon, J. M.; Scott, R. S.; MacDonald, S. M. Distinct characteristics of signal transduction events by histamine-releasing factor/translationally controlled tumor protein (HRF/TCTP)-induced priming and activation of human basophils. *Blood* **2008**, *111* (4), 1789–96.
(52) Gachet, Y.; Tournier, S.; Lee, M.; Lazaris-Karatzas, A.; Poulton, T.; Bommer, U. A. The growth-related, translationally controlled protein P23 has properties of a tubulin binding protein and associates transiently with microtubules during the cell cycle. *J. Cell Sci.* **1999**, *112* (Pt 8), 1257–71.
(53) Burgess, A.; Labbe, J. C.; Vigneron, S.; Bonneaud, N.; Strub, J. M.; Van Dorsselaer, A.; Lorca, T.; Castro, A. Chfr interacts and colocalizes with TCTP to the mitotic spindle. *Oncogene* **2008**, *27*, 5554–5566.
(54) Li, F.; Zhang, D.; Fujise, K. Characterization of fortilin, a novel antiapoptotic protein. *J. Biol. Chem.* **2001**, *276* (50), 47542–9.
(55) Liu, H.; Peng, H. W.; Cheng, Y. S.; Yuan, H. S.; Yang-Yen, H. F. Stabilization and enhancement of the antiapoptotic activity of mcl-1 by TCTP. *Mol. Cell. Biol.* **2005**, *25* (8), 3117–26.
(56) Yang, Y.; Yang, F.; Xiong, Z.; Yan, Y.; Wang, X.; Nishino, M.; Mirkovic, D.; Nguyen, J.; Wang, H.; Yang, X. F. An N-terminal region of translationally controlled tumor protein is required for its antiapoptotic activity. *Oncogene* **2005**, *24* (30), 4778–88.
(57) Hsu, Y. C.; Chern, J. J.; Cai, Y.; Liu, M.; Choi, K. W. Drosophila TCTP is essential for growth and proliferation through regulation of dRheb GTPase. *Nature* **2007**, *445* (7129), 785–8.
(58) Levy, D. E.; Darnell, J. E., Jr. Stats: transcriptional control and biological impact. *Nat. Rev. Mol. Cell Biol.* **2002**, *3* (9), 651–62.
(59) Al Zaid Siddiquee, K.; Turkson, J. STAT3 as a target for inducing apoptosis in solid and hematological tumors. *Cell Res.* **2008**, *18* (2), 254–67.
(60) Germain, D.; Frank, D. A. Targeting the cytoplasmic and nuclear functions of signal transducers and activators of transcription 3 for cancer therapy. *Clin. Cancer Res.* **2007**, *13* (19), 5665–9.
(61) Seita, J.; Asakawa, M.; Ooehara, J.; Takayanagi, S.; Morita, Y.; Watanabe, N.; Fujita, K.; Kudo, M.; Mizuguchi, J.; Ema, H.; Nakauchi, H.; Yoshimoto, T. Interleukin-27 directly induces differentiation in hematopoietic stem cells. *Blood* **2008**, *111* (4), 1903–12.
(62) Alvarez, J. V.; Febbo, P. G.; Ramaswamy, S.; Loda, M.; Richardson, A.; Frank, D. A. Identification of a genetic signature of activated signal transducer and activator of transcription 3 in human tumors. *Cancer Res.* **2005**, *65* (12), 5054–62.
(63) Yu, H.; Kortylewski, M.; Pardoll, D. Crosstalk between cancer and immune cells: role of STAT3 in the tumour microenvironment. *Nat. Rev. Immunol.* **2007**, *7* (1), 41–51.
(64) Turkson, J.; Jove, R. STAT proteins: novel molecular targets for cancer drug discovery. *Oncogene* **2000**, *19* (56), 6613–26.
(65) Deng, J.; Grande, F.; Neamati, N. Small molecule inhibitors of Stat3 signaling pathway. *Curr. Cancer Drug Targets* **2007**, *7* (1), 91–107.

PR100992E